Electrochimica Acta 206 (2016) 374–380

Contents lists available at ScienceDirect

Electrochimica Acta

journal homepage: www.elsevier.com/locate/electacta

# Disordered spinel $LiNi_{0.5}Mn_{1.5}O_4$ cathode with improved rate performance for lithium-ion batteries

Nur Diyana Rosedhi[a], Nurul Hayati Idris[a,*], Md Mokhlesur Rahman[b], M.F. Md Din[c], Jianli Wang[d]

[a] School of Ocean Engineering, Universiti Malaysia Terengganu, 21030 Kuala Terengganu, Terengganu, Malaysia
[b] Institute for Frontier Materials, Deakin University, Waurn Ponds, Victoria 3216, Australia
[c] Department of Electrical & Electronic Engineering, Faculty of Engineering, National Defence University of Malaysia, Kem Sungai Besi, 57000 Kuala Lumpur, Malaysia
[d] Institute for Superconducting and Electronic Materials, University of Wollongong NSW, Australia

ARTICLE INFO

*Article history:*
Received 8 March 2016
Received in revised form 11 April 2016
Accepted 26 April 2016
Available online 27 April 2016

*Keywords:*
$LiNi_{0.5}Mn_{1.5}O_4$
lithium-ion batteries
cathode materials
glycine

ABSTRACT

The high voltage $LiNi_{0.5}Mn_{1.5}O_4$ cathode with a disordered spinel structure is synthesized by a glycine-assisted low-temperature reaction follows by a thermal treatment at 750 °C, 850 °C, and 950 °C for 12 h. Glycine is used as a chelating agent for the first time to build required environment for shaping the precursor of $LiNi_{0.5}Mn_{1.5}O_4$ materials. The microstructure and morphology of the $LiNi_{0.5}Mn_{1.5}O_4$ product are characterized by X-ray diffraction, X-ray photoelectron spectroscopy, scanning electron microscopy, Brunauer-Emmett-Teller, and transmission electron microscopy. The sample prepares at 750 °C reveals small particles with well-defined crystals as confirmed by electron microscopy. Electrochemical results demonstrate that $LiNi_{0.5}Mn_{1.5}O_4$ electrode anneal at 750 °C (compare to other two samples) delivers the highest reversible capacity of 110 mAh $g^{-1}$ at 0.2C after 100 cycles with good rate capability. The enhanced electrochemical performance could be attributed to the smaller particle sizes as well as well-defined crystals which provide a directional and shorter diffusion path length for $Li^+$ transportation within the crystals.



## 1. Introduction

As one of the most attractive green energy resources, lithium-ion batteries (LIBs) have been a major area of interest within the field of power sources and it has been viewed as a great market potential for electric vehicles, cell phones, digital cameras, and laptop computers [1]. Therefore, several goals such as cycling life, energy density, lifetime, and discovering new design for electrode materials that are capable of delivering either high lithium ion storage capacities or high working voltage without undergoing degradation will be researched to fulfill the demands of these applications [2]. Nowadays, LIBs still received enormous attraction among scientists due to excellent cyclic stability, high energy density, fast charge/discharge rate, low toxicity, environmental benign, and good capacity retention compared to other conventional rechargeable devices like nickel cadmium (Ni-Cd) and lead acid (Pb-acid) batteries [3,4]. Currently, LIBs with layered $LiCoO_2$ cathode probably represent the most popular and commercial cathode materials due to its good cyclic stability since its discovery in 1991. However, this cathode material gives some limitations; for example, it exhibits insufficient conductivity and slow lithium diffusivity which lead to failure performance when overcharged [5]. Accordingly, $LiMn_2O_4$ cathode material has been intense in the recent years due to its higher thermal stability at the charge state, fast $Li^+$ diffusivity, low material cost, higher abundance of Mn in the earth, environmentally harmless, ease preparation, and non-toxicity [6,7]. On the other hand, its poor cycling stability and low electronic conductivity lead to rapid capacity fading in the subsequent cycles caused by $Mn^{3+}$ dissolution [7,8] and the Jahn-Teller effect [9,10], which completely limit the LIBs performance to meet higher charge storage. To overcome these issues, researchers have studied the effect on substituting $LiMn_2O_4$ with various elements such as Zn [11], Ni [12], Cr [13], and Co [14]. It was found that doping approaches can enhance its structural stability, consequently improved its cathodic performance [12].

Recently, spinel $LiNi_{0.5}Mn_{1.5}O_4$ is identified as one of the most promising high-voltage cathode materials for the next generation of LIBs due to its high energy density, good rate performance, and

* Corresponding author. Tel.: +60 96683185; fax: +60 96683391.
*E-mail address:* nurulhayati@umt.edu.my (N.H. Idris).

http://dx.doi.org/10.1016/j.electacta.2016.04.152
0013-4686/

good cycling stability with a delivering reversible capacity of more than 100 mAh $g^{-1}$. It has been shown that spinel $Li_4Ti_5O_{12}$ anode couple with high-voltage spinel $LiNi_{0.5}Mn_{1.5}O_4$ cathode could leads to the development of high operating voltage in full cell/battery. These combinations of spinel promote good capacity retention and high rate capability, indicating its promising potential as a suitable candidate for EVs/HEVs or other future applications [15]. Therefore, $LiNi_{0.5}Mn_{1.5}O_4$ itself possesses a dominant plateau at around ~4.7 V according to the oxidation-reduction process of $Ni^{2+}/Ni^{4+}$ and shows better structural stability during the electrochemical process by providing fast $Li^+$ diffusion within the three-dimensional spinel structure [16–19]. From crystallographic point of view, spinel $LiNi_{0.5}Mn_{1.5}O_4$ can form two types of crystal structures: disordered $LiNi_{0.5}Mn_{1.5}O_4$ which is the cubic spinel face-centered (*Fd3m*) and ordered $LiNi_{0.5}Mn_{1.5}O_4$ with a primitive simple cubic crystal (*$P4_332$*), this depends on the ordering of Mn and Ni in the octahedral sites [20–22]. Compared to the ordered one, the disordered spinel exhibits better electrochemical performance mainly with the presence of manganese in the Mn (III) oxidation state, which can be oxidized to Mn (IV) at around 4 V. The presence of redox-active $Mn^{3+}$ enhances electronic conductivity and higher $Mn^{3+}$ ion content also delivers better discharge capacity at higher charge/discharge rates [21,22]. However, electrochemical performances also depend on the conditions of synthesis process involved.

Until now, a significant number of methods have been introduced to prepare $LiNi_{0.5}Mn_{1.5}O_4$ including solid state reaction [23], sol-gel method [24], microwave rapid preparation [25], molten salt method [19], polymer precursor method [12], sonochemical method [26], and so on. Different synthesis processes can result in different properties, structures, morphologies, phase purity, and crystallinity of $LiNi_{0.5}Mn_{1.5}O_4$ [27]. However, the synthesis of high purity $LiNi_{0.5}Mn_{1.5}O_4$ is very challenging as NiO and $Li_xNi_{1-x}O$ usually arise in the final product owing to the oxygen loss at high temperature which deteriorates electrochemical performance. In this work, we first report on the preparation and characterization of high purity disordered spinel $LiNi_{0.5}Mn_{1.5}O_4$ via glycine-assisted solution route at low-temperature reaction. In fact, the important function of glycine as a chelating agent is seen in controlling the precursor's morphology [27]. The addition of glycine during the synthesis process is not just only appears as an organic fuel that can accelerates the decomposition of metal complexes powder, but also assist to inhibit the narrow-sized particles [28,29]. In terms of chemistry, the hydroxyl and amino groups in glycine play an important role in forming an effective complex with metal cations during heating process which help in preventing phase separation in the precursor solution as well as improving the homogeneity of particles [30]. Other chelating agents such as citric acid [28], adipic acid [30], and gelatin [31] were also have been introduced as a starting precursor in synthesizing many materials. For example, citric acid has been used in synthesizing $Li_4Ti_5O_{12}$ material as reported by Hao et al. [28]. The addition of citric acid significantly allows the precursor in gel solution to disperse well with good stoichiometry control. During sintering, citric acid may also act as protector to protect particle growth from agglomerate to each other, leading to the homogenous particle. Homogeneous distribution of fine particles could be the key issue attained by using glycine as a chelating agent that enhances electrochemical performance of $LiNi_{0.5}Mn_{1.5}O_4$ cathode.

## 2. Experimental

### 2.1. Synthesis of spinel $LiNi_{0.5}Mn_{1.5}O_4$

To prepare $LiNi_{0.5}Mn_{1.5}O_4$, 0.65 g of $NiCl_2$ (Aldrich, 98%), 2.97 g of $MnCl_2.4H_2O$ (Sigma-Aldrich, 99%), 0.42 g of $LiOH{\cdot}H_2O$ (Sigma-Aldrich, 99%), and 2.50 g of glycine (Sigma, 99%) were homogeneously dissolved in deionized water. The solution was then heated at 90 °C for 8 h under vacuum until blue suspension was formed. The as-obtained precursor was heat-treated at 580 °C for 5 h and then further heated at 750 °C, 850 °C, and 950 °C, respectively for 12 h in air to yield the final products. The synthesized powders obtained were marked as S580, S750, S850, and S950, respectively.

### 2.2. Materials characterization

The structure and phase composition of $LiNi_{0.5}Mn_{1.5}O_4$ samples were characterized by XRD (Rigaku Miniflex II) with Cu-Kα radiation from 5° to 80° at a scan rate of 0.2° $min^{-1}$. In order to figure out of the real structure of the samples, Rietveld refinement was carried out using Fullprof software (version 5.60). XPS was performed to determine the average oxidation states of Ni and Mn in the materials. XPS spectra were collected on the Axis Ultra DLD XPS, Kratos. The morphology features and particle size of the materials were observed by SEM (JEOL JSM-6360LA) and TEM (JEOL JEM-2100F) with an accelerating voltage of 200 kV. The specific surface areas of the samples were calculated according to the BET method using surface area analyzer (Micromeritics ASAP 2020).

### 2.3. Electrochemical measurements

To prepare the electrodes, active materials were mixed with carbon black (Aldrich, 99.95%) and sodium carboxymethylcellulose (CMC) (Sigma-Aldrich) binder in deionized water as a solvent with a weight ratio of 75:20:5, respectively. After mixing thoroughly, the slurry was pasted onto a thin aluminum foil ($1 \times 1$ $cm^2$ in size) current collector and the coated electrodes were dried under vacuum at 100 °C for 5 h. The weight of active material on each electrode was ~1.5 mg. The coin-type cell (CR2032) was assembled in an argon-filled glove box by pressing the prepared cathode together with the lithium foil as the counter electrode separated by a porous polypropylene film as a separator. 1 M of $LiPF_6$ dissolved in ethylene carbonate (EC) and diethyl carbonate (DEC) (1:1 by volume) was used as the electrolyte. Galvanostatic charge-discharge tests were performed in a voltage range of 3.0–4.9 V with different current densities using Neware battery testing system. The cyclic voltammetry (CV) tests were scanned between 3.0–4.9 V at a scan rate of 0.3 mV $s^{-1}$ using CHI650D electrochemical workstation.

## 3. Results and discussion

Fig. 1 presents the XRD patterns and the Rietveld refinement fits of the $LiNi_{0.5}Mn_{1.5}O_4$ samples prepared at different temperatures for 12 h. All patterns were confirmed as a typical cubic spinel structure and the diffraction peaks at 18.73°, 30.57°, 36.41°, 38.08°, 44.39°, 48.45°, 58.54°, 64.52°, 67.81°, 76.35°, and 77.42° corresponded to the crystal planes of (111), (220), (311), (222), (400), (331), (511), (440), (531), (533), and (622), respectively, in which were well-matched to the conventional spinel of $LiNi_{0.5}Mn_{1.5}O_4$ with a *Fd3m* space group (JCPDS No. 80-2162). As shown in the results, sample S750 and S850 exhibited cubic spinel structure without any peaks of impurities. It was observed that sample S750 exhibited a very sharp and high intensity in the XRD reflections due to the high crystallinity of the sample which is beneficial for high discharge capacity and good stability [16,32]. No other impurities peaks were detected for the sample S850, however, the reflection peaks started to slightly broaden. Furthermore, some minor residue peaks at 37.46°, 43.43°, and 63.09° were detected for sample S950 as impurity structure was formed (NiO) around 4.20 wt%, suggesting the occurrence of oxygen loss when

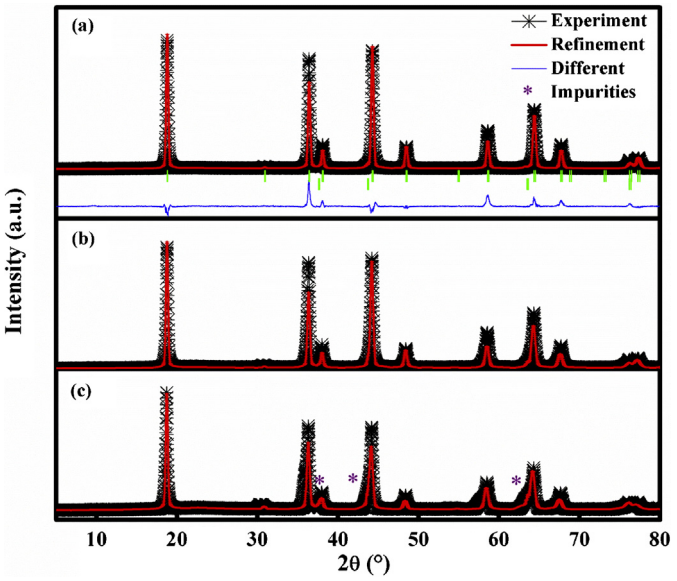


**Fig. 1.** Rietveld refinement fits of the XRD data for the samples: (a) S750, (b) S850, and (c) S950. The green markers for the crystallographic structures (top for $LiNi_{0.5}Mn_{1.5}O_4$ phase and bottom for NiO) are indicated. (For interpretation of the references to color in this figure legend, the reader is referred to the web version of this article.)

the temperature goes up. In addition, the full width at half maximum (FWHM) increased as calcination temperatures increased from 750 °C to 950 °C. The crystallite sizes for samples S750, S850, and S950 were 29.45, 28.89, and 27.27 nm, respectively, calculated using the Scherrer formula as shown in Eq. (1).

$$L = \frac{k\lambda}{\beta\cos\theta} \quad (1)$$

Here, $L$ is the crystallite size of the particle, $k$ is the constant (0.9394), $\lambda$ is the X-ray wavelength of Cu-kα radiation (1.5148 Å), β is the full width at half maximum of the major XRD peak in radian and $\theta$ is the angle of diffraction.

The details of lattice parameters, $a$ of the spinel phase are listed in Table 1. The lattice parameter increased simultaneously with the increase of calcination treatment from 8.1828 Å for S750 to 8.2075 Å for S950, respectively. This phenomenon may occur due to the radius of $Mn^{3+}$ (0.6500 Å) which is larger than that of small $Mn^{4+}$ (0.5300 Å); this means oxygen loss will become more serious and more $Mn^{3+}$ concentration will appear in the samples, especially when the temperature is increased [33,34]. However, the lattice parameter is quite larger for all samples than the previous reports (8.1724 Å) [25]. This could be due to different synthesis conditions and different precursors used.

XPS experiments were carried out to estimate the actual amount of Mn and Ni components in the sample S750. The fitted Ni $2p_{3/2}$ and Mn $2p_{3/2}$ XPS peaks of pristine $LiNi_{0.5}Mn_{1.5}O_4$ sample are shown in Fig. 2. Fig. 2a shows that the binding energy of $Ni^{2+}$ and

**Table 1**
Rietveld refinement results for the samples S750, S850, and S950, respectively. The standard errors derived from the refinements are also listed in lattices columns.

| Sample | | $a$ (Å) | Bragg $R_{factor}$ (%) | $R_{F\ factor}$ (%) | $\chi^2$ |
|---|---|---|---|---|---|
| S750 | $LiNi_{0.5}Mn_{1.5}O_4$ | 8.1828(3) | 6.8 | 8.5 | 4.28 |
| S850 | $LiNi_{0.5}Mn_{1.5}O_4$ | 8.1966(2) | 8.8 | 9.8 | 5.79 |
| S950 | $LiNi_{0.5}Mn_{1.5}O_4$ | 8.2075(5) | 16.6 | 10.9 | 7.86 |
| | NiO | 4.1405(2) | 4.9 | 3.6 | |

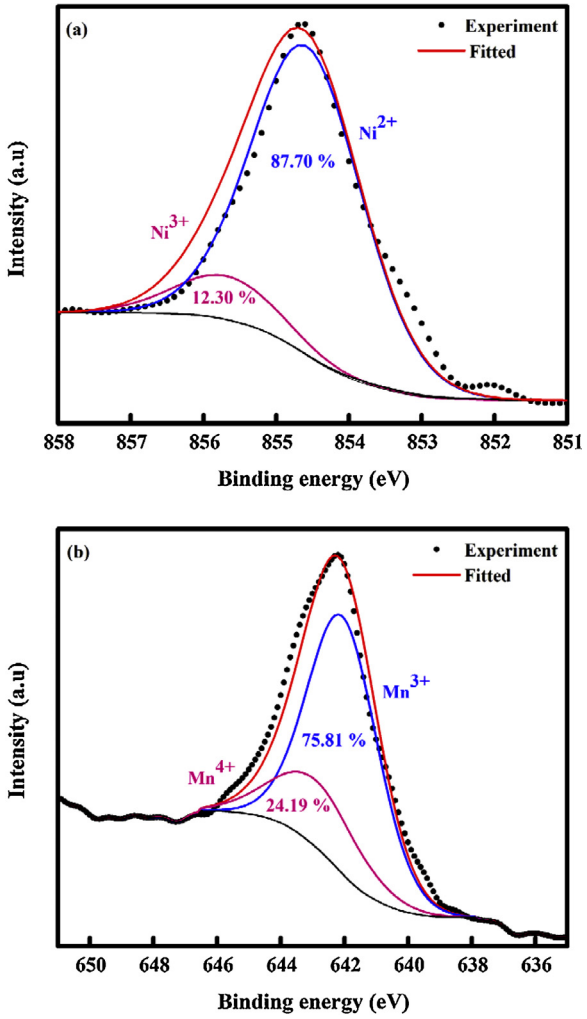


**Fig. 2.** X-ray photoelectron spectra of Ni $2p_{3/2}$ and Mn $2p_{3/2}$ peaks for the sample S750.

$Ni^{3+}$ in Ni $2p_{3/2}$ were located at ~854.5 and ~855.8 eV, respectively. The increase of binding energy in Ni $2p_{3/2}$ is likely owing to the conversion of partial oxidation from $Ni^{2+}$ to $Ni^{3+}$. Otherwise, as shown in Fig. 2b, the Mn $2p_{3/2}$ binding energy was slightly negatively shifted to ~642.3 eV, which suggests that $Mn^{4+}$ is partially reduced to $Mn^{3+}$. The trace amount of $Mn^{3+}$ existed in this sample as seen in Table 2, which confirms that this sample belongs to the *Fd3m* structure, where Ni and Mn ions are distributed randomly in the 16*d* sites. The appearance of $Mn^{3+}$ in this sample may be due to oxygen deficiency formed in the powder surface caused by the exposure to air during calcination process [35].

SEM investigations of the samples are displayed in Fig. 3. A significant morphological change was observed as the calcination temperature increased. The average particle sizes for samples S750, S850, and S950 were 3.52, 4.22, and 4.46 μm, respectively. Fig. 3a shows perfect octahedron shape of the sample S750 calcined at 750 °C. However, the corner of the octahedron tended to shrink for sample S850 calcined at 850 °C (Fig. 3b). No more octahedron shape existed for the sample S950 calcined at 950 °C. The corner became flattened, giving rise to new facets, made the crystals increase in size and formed dodecahedron shape (Fig. 3c). A special crystal growth behavior was observed in all samples in the presence of glycine which led to control the morphology, thus forming a uniform shape. In this way, it hinders

**Table 2**
Ni $2p_{3/2}$ and Mn $2p_{3/2}$ peak positions and cations distribution in the sample S750.

| Sample | Binding energy position (eV) | | Ni $2p_{3/2}$ atomic concentration (%) | | Mn $2p_{3/2}$ atomic concentration (%) | |
|---|---|---|---|---|---|---|
| | Ni $2p_{3/2}$ | Mn $2p_{3/2}$ | $Ni^{2+}$ | $Ni^{3+}$ | $Mn^{3+}$ | $Mn^{4+}$ |
| S750 | 854.70 | 642.30 | 87.70 | 12.30 | 75.81 | 24.19 |

the stage partition and leads to homogenized sized particles during thermal decomposition [30].

BET study was also applied to calculate the specific surface area of the samples. The surface areas of the samples were calculated to be approximately 1.69, 1.87, and 2.00 $m^2 g^{-1}$ for the samples S750, S850, and S950, respectively. The highest surface area for the sample S950 was a result from the increasing number of facets in the polyhedral crystals, as confirmed by the SEM analysis. To obtain the information concerning structural and morphological evolution of the sample S750, TEM measurements were carried out (Fig. 4). Bright-field imaging of the sample revealed dense agglomerates of crystalline $LiNi_{0.5}Mn_{1.5}O_4$ (Fig. 4a). A HRTEM image of the crystal is shown in Fig. 4b. The marked *d*-spacing of 0.47 nm corresponded well with that of (111) planes of spinel $LiNi_{0.5}Mn_{1.5}O_4$. The fast Fourier transform (FFT) pattern of the region in Fig. 4a is shown in Fig. 4c, which clearly revealed the crystalline nature of spinel $LiNi_{0.5}Mn_{1.5}O_4$.

A series of electrochemical measurements were performed to investigate the cathode performance of the electrodes. Fig. 5a compares the cycling performance of the 3 electrodes at a current density of 0.2C up to 100 cycles within the voltage range of 3.0–4.9 V. S750 electrode exhibited higher discharge capacity of 110 mAh $g^{-1}$ in the first cycle and the capacity retention was 101 mAh $g^{-1}$ after 100 cycles. In the case of S850 and S950 electrodes, the capacity retention was 94 mAh $g^{-1}$ for S850 and 73 mAh $g^{-1}$ for S950 electrodes. Lower discharge capacity of both S850 and S950 electrodes (compared to S750 electrode) is believed to initiate from the instability reaction between active material and electrolyte, corresponding to the larger surface area from BET analysis [36,37]. However, the capacity fading behavior was noticed in all electrodes. The reversible capacities at different charge/discharge rates are displayed in Fig. 5b. At the $10^{th}$ cycle, S750 electrode delivered a high reversible capacity of 110 mAh $g^{-1}$ at a rate of 0.2C, whereas it was 107 mAh $g^{-1}$ and 76 mAh $g^{-1}$ for S850 and S950 electrodes, respectively. Even at high current rates of 0.4, 0.6, 0.8, and 1C, S750 electrode still able to deliver maximum reversible capacities of 104, 98, 94, and 90 mAh $g^{-1}$ at the $10^{th}$ cycle, respectively. When the current was turned back to 0.2C after

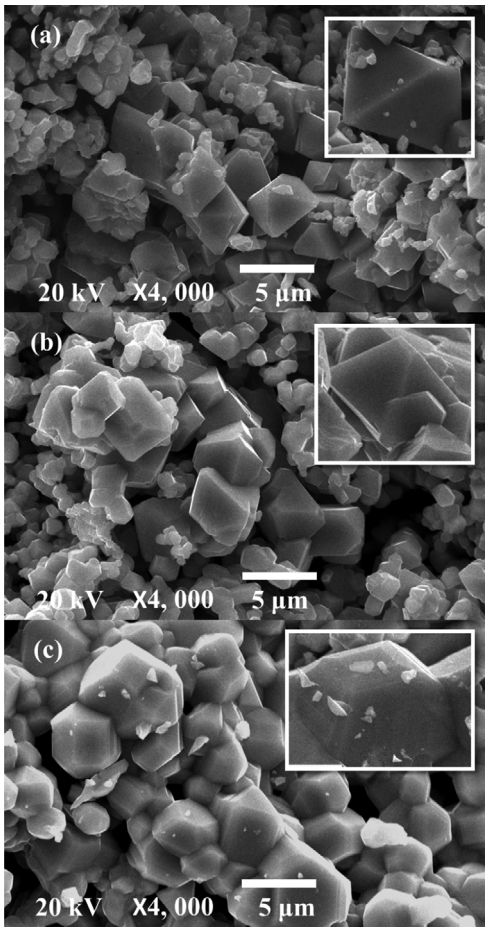


**Fig. 3.** SEM images of samples (a) S750, (b) S850, and (c) S950. Inset: the enlarge images of a–c, respectively.

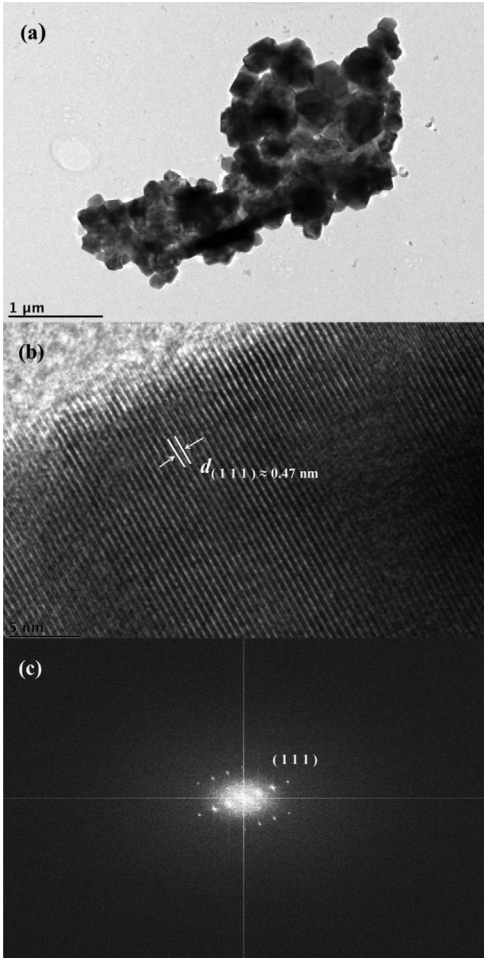


**Fig. 4.** TEM images of sample S750: (a) low magnification image, (b) HRTEM image of the crystal, and (c) FFT pattern.

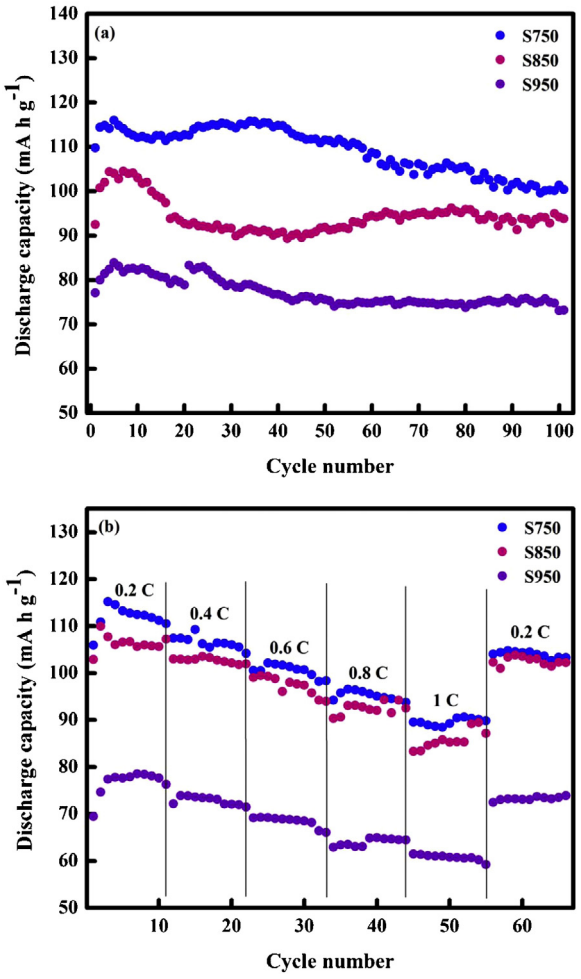


**Fig. 5.** (a) Cycling performance up to 100 cycles at 0.2C rate and (b) consecutive cycling performance at different current rates, ranging from low to very high.

being exposed to different charge-discharge rates, S750 electrode exhibited a reasonable capacity recovery, which implies better rate performance of the electrode. On the other hand, consecutive cycling performance of S850 and S950 electrodes was unsatisfactory. It is convinced that smaller particle size of S750 electrode significantly enhances the rate capability by providing shorter $Li^+$ ion diffusion path length [16,36].

Galvanostatic charge-discharge profiles of the electrodes measured at 0.2C within the voltage range of 3.0–4.9 V are shown in Fig. 6a–c. At the 1st cycle, the electrodes deliver higher charge capacity which could probably related to the formation of electrolyte oxidation on the electrode surface [12]. During discharge, it was very obvious that all electrodes exhibited a long plateau around ~4.6 V, which is ascribed to the nickel oxidation from $Ni^{2+}$ to $Ni^{3+}$. Apparently, the redox of nickel ions mainly contributes to the ion insertion/extraction within the electrode. Obviously, S750 electrode has a long plateau, suggesting its ability to store more capacity during discharge process than others. A short plateau at around ~3.8 V was detected in all electrodes which corresponded to the redox couples of $Mn^{3+}/Mn^{4+}$. However, S750 electrode committed the shortest plateau at 3.8 V for all the three cycles, suggesting the lowest amount of $Mn^{3+}$ content in the sample, which is consistent with the Rietveld refinement result. In contrary, S950 electrode exhibited the longest plateau at 3.8 V (Fig. 6c), suggesting more presence of $Mn^{3+}$ in the sample which deteriorate the electrochemical performance. Xue et al. [16] have reported that a higher content of $Mn^{3+}$ is harmful to the cell's activity due to strain from the Jahn-Teller distortion of $Mn^{3+}$ and the dissolution of $Mn^{2+}$ into the electrolyte resulted from the unstable reaction of $Mn^{3+}$. To get further information about electrochemical activity, CV measurements were performed at a scan rate of 0.3 mV $s^{-1}$. Fig. 6d–f show the cyclic voltammetry curves of S750, S850, and S950 electrodes which were consistent with their discharge profiles curves. As mentioned before, each electrode has a dominant reduction peak which was noticed at around ~4.6 V, corresponding to $Ni^{2+}/Ni^{3+}$, while the small peak at around 3.8 V was associated with $Mn^{3+}/Mn^{4+}$ in the discharge process. Clearly, all electrodes have much sharper peak at ~4.6 V than the peak at 3.8 V, suggesting that $Ni^{2+}/Ni^{3+}$ redox couples are totally responsible for overall electrochemical performance. In the first cycle, S750 electrode promoted the smallest value (0.26 V) of potential difference than the electrodes of S850 (0.27 V) and S950 (0.29 V), and then it was further confirmed that S750 electrode favored efficient $Li^+$ diffusivity and higher reversibility of electrochemical reaction [21].

It is suggested that high crystallinity, homogeneity, and uniform morphology are the key factors to achieve an improved cycling behavior of spinel $LiNi_{0.5}Mn_{1.5}O_4$ cathode. The presence of impurities in the sample simply hampers their electrochemical performance as impurities are able to block the $Li^+$ pathway in the material. No obvious impurity peaks have been detected in the samples except S950. The sample S750 presented a good cycling behavior which is attributed to the crystallinity, small particle size, homogeneity, and uniform morphology. Samples with higher surface area lead to increase the number of facets and increase the challenges to achieve optimum capacity which is mainly caused by the inhibition of surface contact between electrode and electrolyte and finally reduces the electric contact between $LiNi_{0.5}Mn_{1.5}O_4$ and current collector [36]. On the other hand, particles with larger size showed distinct disadvantages; a longer time is needed to transfer $Li^+$ into the core of the particles and faces diffusion limitation of $Li^+$ within a single large particle [38]. It is important to highlight that the use of glycine as a chelating agent gives advantages to the precursor to grow in a required direction, thus developing a well-crystallized octahedral particles [27]. Interestingly, the chelating agent itself generally offers good contacts between homogenous particles which improve the conductivity between particle-to-particle connections [39]. Hence, a well-crystallized phase pure morphology is beneficial for maximum extraction/insertion of $Li^+$ and the enhancement of conductivity. Further research is necessary to improve the cyclability of the lithium-ion batteries and the key parameters that control the performance of high-voltage $LiNi_{0.5}Mn_{1.5}O_4$ is still a challenge. Therefore, ways to improve the cyclability may consist in increasing the specific surface area by producing nanosized $LiNi_{0.5}Mn_{1.5}O_4$. Another strategy to achieve better capacity and cyclability is by substituting other elements such as Ti, Fe, Cr and Mg into the spinel or surface coating with $Al_2O_3$, ZnO, and $V_2O_5$.

## 4. Conclusion

Spinel $LiNi_{0.5}Mn_{1.5}O_4$ cathode materials were successfully synthesized via a simple low-temperature reaction followed by thermal treatment which used glycine as the chelating agent. A set of characterization techniques of X-ray diffraction (XRD), X-ray photoelectron spectroscopy (XPS), Brunauer-Emmett-Teller (BET), scanning electron microscopy (SEM) and transmission electron microscopy (TEM) were employed to identify the phases and structures, chemical composition, surface area, and morphology of the materials produced. XRD patterns demonstrated that samples prepared at 750 °C exhibited high crystallinity and high purity compared to the other samples prepared at 850 °C and 950 °C. The

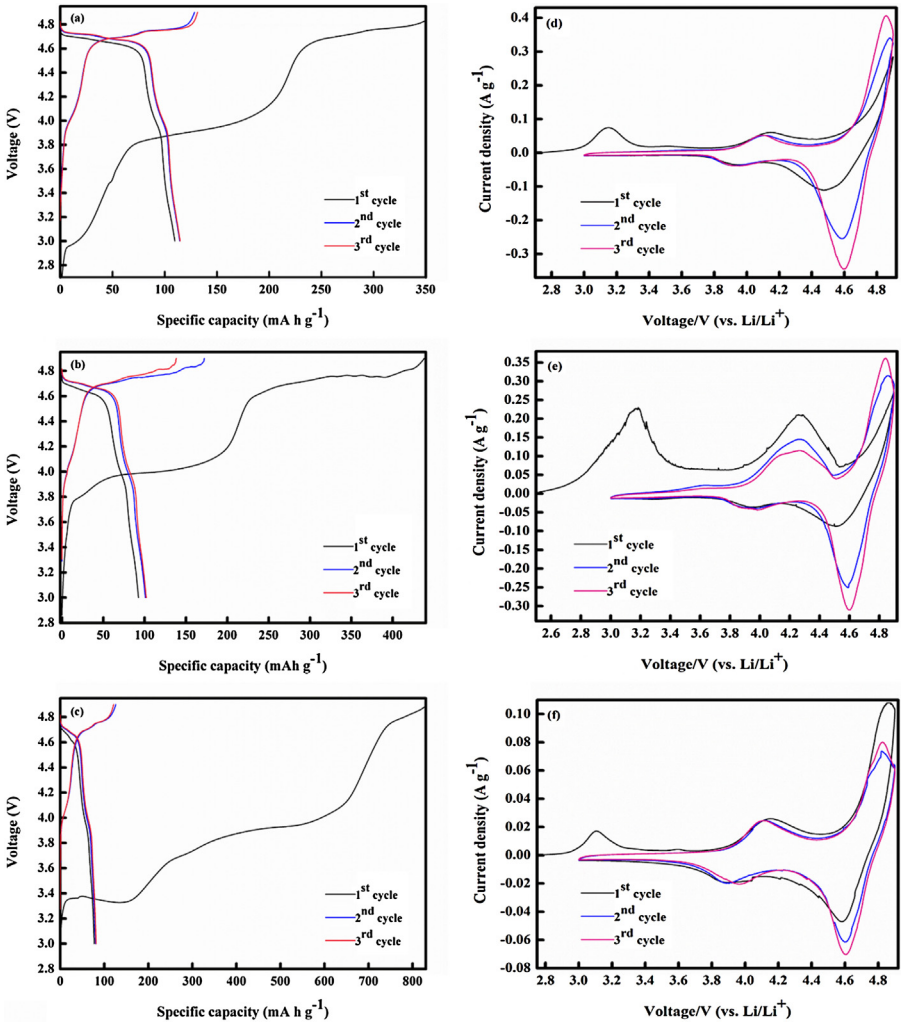


**Fig. 6.** Charge-discharge profiles of (a) S750, (b) S850, and (c) S950 electrodes, and (d–f) CV of (d) S750, (e) S850, and (f) S950 electrodes for the 1st, 2nd and 3rd cycles.

actual amount of Mn and Ni components and their distribution in the sample prepared at 750 °C were confirmed by XPS analysis. The spinel obtained at 750 °C possessed octahedron morphology with micrometer-sized particles (smaller in size than the other two samples). Heat treatment at 850 °C and 950 °C partially destroyed the crystallite alignment and increased the particles size. TEM analysis was carried out to reveal the crystalline nature of the $LiNi_{0.5}Mn_{1.5}O_4$ prepared at 750 °C. The highest surface area was measured for the sample prepared at 950 °C because of increasing number of facets in the polyhedral crystals, as was confirmed by the SEM analysis. The demonstrated electrochemical performance of $LiNi_{0.5}Mn_{1.5}O_4$ obtained at 750 °C was superior to those of $LiNi_{0.5}Mn_{1.5}O_4$ obtained at 850 °C and 950 °C, respectively. The improved electrochemical performance of $LiNi_{0.5}Mn_{1.5}O_4$ obtained at 750 °C is attributed to high crystallinity, high purity, smaller particle size, and uniform morphology of the product.

## Acknowledgements

Financial support was provided by the Ministry of Higher Education, Malaysia through a Fundamental Research Grant Scheme (FRGS) (Vote no. 59323) and MyBrain15 scholarship sponsored to the student is gratefully acknowledged.

## References

[1] Y. Nishi, Lithium ion secondary batteries; past 10 years and the future, J. Power Sources 100 (2001) 101–106.
[2] S.-G. Hwang, G.-O.K. Kim, S.-R. Yun, K.-S. Ryu, NiO nanoparticles with plate structure grown on graphene as fast charge–discharge anode material for lithium ion batteries, Electrochim. Acta 78 (2012) 406–411.
[3] Z. Zeng, H. Zhao, J. Wang, P. Lv, T. Zhang, Q. Xia, Nanostructured $Fe_3O_4$@C as anode material for lithium-ion batteries, J. Power Sources 248 (2014) 15–21.
[4] Q. Zhou, Z. Zhao, Z. Wang, Y. Dong, X. Wang, Y. Gogotsi, J. Qiu, Low temperature plasma synthesis of mesoporous $Fe_3O_4$ nanorods grafted on reduced graphene oxide for high performance lithium storage, Nanoscale 6 (2014) 2286–2291.
[5] E. Han, Q. Jing, L. Zhu, G. Zhang, S. Ma, The effects of sodium additive on $Li_{1.17}Ni_{0.10}Co_{0.10}Mn_{0.63}O_2$ for lithium ion batteries, J. Alloys Compd. 618 (2015) 629–634.
[6] M. Aklalouch, J.M. Amarilla, R.M. Rojas, I. Saadoune, J.M. Rojo, Chromium doping as a new aproach to improve the cycling performance at high temperature of 5 V $LiNi_{0.5}Mn_{1.5}O_4$-based positive electrode, J. Power Sources 185 (2008) 501–511.
[7] Y.-L. Ding, J. Xie, G.-S. Cao, T.-J. Zhu, H.-M. Yu, X.-B. Zhao, Single-crystalline $LiMn_2O_4$ nanotubes synthesized via template-engaged reaction as cathodes for high-power lithium ion batteries, Adv. Funct. Mater. 21 (2011) 348–355.
[8] J.-S. Chen, L.-F. Wang, B.-J. Fang, S.-Y. Lee, R.-Z. Guo, Rotating ring–disk electrode measurements on Mn dissolution and capacity losses of spinel electrodes in various organic electrolytes, J. Power Sources 157 (2006) 515–521.
[9] S.-W. Lee, K.-S. Kim, H.-S. Moon, J.-P. Lee, H.-J. Kim, B.-W. Cho, W.-I. Cho, J.-W. Park, Electrochemical and structural characteristics of metal oxide-coated

lithium manganese oxide (spinel type): Part I. In the range of 2.5–4.2 V, J. Power Sources 130 (2004) 227–232.
[10] D. Shu, K. Gopu, K.-B. Kim, K.S. Ryu, S.H. Chang, Surface modification of $LiMn_2O_4$ thin films at elevated temperature, Solid State Ionics 160 (2003) 227–233.
[11] D. Arumugam, G.P. Kalaignan, K. Vediappan, C.W. Lee, Synthesis and electrochemical characterizations of nano-scaled Zn doped $LiMn_2O_4$ cathode materials for rechargeable lithium batteries, Electrochim. Acta 55 (2010) 8439–8444.
[12] M.V. Reddy, H.Y. Cheng, J.H. Tham, C.Y. Yuan, H.L. Goh, B.V.R. Chowdari, Preparation of $Li(Ni_{0.5}Mn_{1.5})O_4$ by polymer precursor method and its electrochemical properties, Electrochim. Acta 62 (2012) 269–275.
[13] Y.-P. Fu, Y.-H. Su, S.-H. Wu, C.-H. Lin, $LiMn_{2-y}M_yO_4$ (M = Cr, Co) cathode materials synthesized by the microwave-induced combustion for lithium ion batteries, J. Alloys Compd. 426 (2006) 228–234.
[14] A. Sakunthala, M.V. Reddy, S. Selvasekarapandian, B.V.R. Chowdari, P.C. Selvin, Synthesis of compounds, $Li(MMn_{11/6})O_4$ (M = $Mn_{1/6}$ $Co_{1/6,}$ ($Co_{1/12}Cr_{1/12}$), ($Co_{1/12}Al_{1/12}$), ($Cr_{1/12}Al_{1/12}$)) by polymer precursor method and its electrochemical performance for lithium-ion batteries, Electrochim. Acta 55 (2010) 4441–4450.
[15] H.F. Xiang, X. Zhang, Q.Y. Jin, C.P. Zhang, C.H. Chen, X.W. Ge, Effect of capacity matchup in the $LiNi_{0.5}Mn_{1.5}O_4/Li_4Ti_5O_{12}$ cells, J. Power Sources 183 (2008) 355–360.
[16] Y. Xue, Z. Wang, F. Yu, Y. Zhang, G. Yin, Ethanol-assisted hydrothermal synthesis of $LiNi_{0.5}Mn_{1.5}O_4$ with excellent long-term cyclability at high rate for lithium-ion batteries, J. Mater. Chem. A 2 (2014) 4185–4191.
[17] S.H. Park, S.W. Oh, S.H. Kang, I. Belharouak, K. Amine, Y.K. Sun, Comparative study of different crystallographic structure of $LiNi_{0.5}Mn_{1.5}O_{4-\delta}$ cathodes with wide operation voltage (2.0–5.0 V), Electrochim. Acta 52 (2007) 7226–7230.
[18] M. Zhang, J. Wang, Y. Xia, Z. Liu, Microwave synthesis of spherical spinel $LiNi_{0.5}Mn_{1.5}O_4$ as cathode material for lithium-ion batteries, J. Alloys Compd. 518 (2012) 68–73.
[19] J.H. Kim, S.T. Myung, Y.K. Sun, Molten salt synthesis of $LiNi_{0.5}Mn_{1.5}O_4$ spinel for 5 V class cathode material of Li-ion secondary battery, Electrochim. Acta 49 (2004) 219–227.
[20] J. Chong, S. Xun, X. Song, G. Liu, V.S. Battaglia, Surface stabilized $LiNi_{0.5}Mn_{1.5}O_4$ cathode materials with high-rate capability and long cycle life for lithium ion batteries, Nano Energy 2 (2013) 283–293.
[21] C.J. Jafta, M.K. Mathe, N. Manyala, W.D. Roos, K.I. Ozoemena, Microwave-assisted synthesis of high-voltage nanostructured $LiMn_{1.5}Ni_{0.5}O_4$ spinel: Tuning the $Mn^{3+}$ content and electrochemical performance, ACS Appl. Mater. Interfaces 5 (2013) 7592–7598.
[22] X. Ma, B. Kang, G. Ceder, High rate micro-sized ordered $LiNi_{0.5}Mn_{1.5}O_4$, J. Electrochem. Soc. 157 (2010) A925–A931.
[23] X.Y. Feng, C. Shen, X. Fang, C.H. Chen, Synthesis of $LiNi_{0.5}Mn_{1.5}O_4$ by solid-state reaction with improved electrochemical performance, J. Alloys Compd. 509 (2011) 3623–3626.
[24] S. Niketic, M. Couillard, D. MacNeil, Y. Abu-Lebdeh, Improving the performance of high voltage $LiMn_{1.5}Ni_{0.5}O_4$ cathode material by carbon coating, J. Power Sources 271 (2014) 285–290.
[25] P. Gao, L. Wang, L. Chen, X. Jiang, J. Pinto, G. Yang, Microwave rapid preparation of $LiNi_{0.5}Mn_{1.5}O_4$ and the improved high rate performance for lithium-ion batteries, Electrochim. Acta 100 (2013) 125–132.
[26] P. Sivakumar, P.K. Nayak, B. Markovsky, D. Aurbach, A. Gedanken, Sonochemical synthesis of $LiNi_{0.5}Mn_{1.5}O_4$ and its electrochemical performance as a cathode material for 5 V Li-ion batteries, Ultrason. Sonochem. 26 (2015) 332–339.
[27] Y.Q. Qiao, J.P. Tu, X.L. Wang, J. Zhang, Y.X. Yu, C.D. Gu, Self-assembled synthesis of hierarchical waferlike porous Li-V-O composites as cathode materials for lithium ion batteries, J. Phys. Chem. C 115 (2011) 25508–25518.
[28] Y.-j. Hao, Q.-y. Lai, D.-q. Liu, Z.-u. Xu, X.-y. Ji, Synthesis by citric acid sol–gel method and electrochemical properties of $Li_4Ti_5O_{12}$ anode material for lithium-ion battery, Mater. Chem. Phys. 94 (2005) 382–387.
[29] S.-k. Zhong, Y. Wang, J.-q. Liu, J. Wang, Synthesis of $LiMnPO_4$/C composite material for lithium ion batteries by sol-gel method, Transactions of Nonferrous Metals Society of China 22 (2012) 2535–2540.
[30] T.-F. Yi, C.-L. Hao, C.-B. Yue, R.-S. Zhu, J. Shu, A literature review and test: Structure and physicochemical properties of spinel $LiMn_2O_4$ synthesized by different temperatures for lithium ion battery, Synth. Met. 159 (2009) 1255–1260.
[31] M. Mo, C. Ye, K. Lai, Z. Huang, L. Zhu, G. Ma, H. Chen, K.S. Hui, Gelatin-assisted synthesis of $LiNi_{0.5}Mn_{1.5}O_4$ cathode material for 5 V lithium rechargeable batteries, Appl. Surf. Sci. 276 (2013) 635–640.
[32] Y.-K. Sun, K.-H. Lee, S.-I. Moon, I.-H. Oh, Effect of crystallinity on the electrochemical behaviour of spinel $Li_{1.03}Mn_2O_4$ cathode materials, Solid State Ionics 112 (1998) 237–243.
[33] Y.-P. Zeng, X.-l. Wu, P. Mei, L.-N. Cong, C. Yao, R.-S. Wang, H.-M. Xie, L.-Q. Sun, Effect of cationic and anionic substitutions on the electrochemical properties of $LiNi_{0.5}Mn_{1.5}O_4$ spinel cathode materials, Electrochim. Acta 138 (2014) 493–500.
[34] H.Y. Xu, S. Xie, N. Ding, B.L. Liu, Y. Shang, C.H. Chen, Improvement of electrochemical properties of $LiNi_{0.5}Mn_{1.5}O_4$ spinel prepared by radiated polymer gel method, Electrochim. Acta 51 (2006) 4352–4357.
[35] J.H. Lee, K.J. Kim, Structural and electrochemical evolution with post-annealing temperature of solution-based $LiNi_{0.5}Mn_{1.5}O_4$ thin-film cathodes for microbatteries with cyclic stability, Electrochim. Acta 137 (2014) 169–174.
[36] A.S. Arico, P. Bruce, B. Scrosati, J.-M. Tarascon, W. Van Schalkwijk, Nanostructured materials for advanced energy conversion and storage devices, Nat. Mater. 4 (2005) 366–377.
[37] X. Zhu, X. Li, Y. Zhu, S. Jin, Y. Wang, Y. Qian, Porous $LiNi_{0.5}Mn_{1.5}O_4$ microspheres with different pore conditions: Preparation and application as cathode materials for lithium-ion batteries, J. Power Sources 261 (2014) 93–100.
[38] T. Drezen, N.-H. Kwon, P. Bowen, I. Teerlinck, M. Isono, I. Exnar, Effect of particle size on $LiMnPO_4$ cathodes, J. Power Sources 174 (2007) 949–953.
[39] S. Kandhasamy, P. Singh, S. Thurgate, M. Ionescu, D. Appadoo, M. Minakshi, Olivine-type cathode for rechargeable batteries: Role of chelating agents, Electrochim. Acta 82 (2012) 302–308.